Laser and Particle Beams (2004), *22*, 253–259. Printed in the USA.
Copyright © 2004 Cambridge University Press 0263-0346/04 $16.00
DOI: 10.1017/S0263034604223072

Ray-tracing simulations of a bent crystal X-ray optics for imaging using laser–plasma X-ray sources

L. LABATE,[1,2] M. GALIMBERTI,[1] A. GIULIETTI,[1] D. GIULIETTI,[1,3] L.A. GIZZI,[1]
P. KÖSTER,[1] S. LAVILLE,[1] AND P. TOMASSINI[1]

[1]Intense Laser Irradiation Laboratory–IPCF (CNR) Pisa, Italy
[2]Dipartimento di Fisica–Università di Bologna, Bologna, Italy
[3]Dipartimento di Fisica–Università di Pisa, and INFM, sezione di Pisa, Italy

(RECEIVED 1 November 2003; ACCEPTED 17 February 2004)

Abstract

Ray-tracing simulations of an optical X-ray system based on a spherically bent crystal operating in Bragg configuration for monochromatic projection imaging of thin samples are presented, obtained using a code developed for that purpose. The code is particularly suited for characterizing experimental arrangements routinely used with laser-produced plasma X-ray sources. In particular, the spatial resolution of the imaging system was investigated and a careful study of the complex pattern of the X-ray backlighting beam was performed.

Keywords: Plasma X-ray emission; Ray-tracing simulations; X-ray imaging; X-ray optics

1. INTRODUCTION

Laser-produced plasmas are currently recognized as bright and versatile pulsed sources of X-ray radiation for a wide range of applications, having a pulse duration ranging from the nanosecond down to the 100-fs scale, sizes of the order of 10–100 μm and repetition rate of 10–100 Hz (see, e.g., Giulietti & Gizzi, 1998, and references therein).

The X-ray spectrum from laser plasmas consists of incoherent radiation due to Bremsstrahlung as well as line emission from high charge state ions, which is particularly useful when using plasmas produced at lower intensities (Marzi *et al*., 2000; Labate *et al*., 2002). More recently, characteristic radiation emission (mainly K_α and K_β) from the cold target material (see, e.g., Von Der Linde *et al*., 2001, and references therein), whose generation is particularly efficient at laser intensities of the order of 10^{17} W/cm^2 or higher with hundredths of femtosecond duration (Bastiani *et al*., 1997; Reich *et al*., 2000), has been studied and exploited for applications.

When dealing with such a kind of broad-band radiation, a suitable X-ray optics is used when a monochromatic X-ray beam is needed. Using a monochromatic X-ray beam is a crucial issue to enhance the contrast in X-ray imaging applications (Burattini *et al*., 1990) and to explore the so-called water-window region. Also, a monochromatic X-ray beam is a prerequisite in order to use the so-called differential absorption imaging technique (Dix, 1995). This technique is a powerful tool to search for specific elements in a sample by using X-ray radiography. The technique has been proposed for the detection of small concentrations of contrast agents in biological and medical applications. It is currently under study for clinical application in coronary angiography. Such kinds of studies are carried out using either monochromatized synchrotron sources (Suortti & Thomlinson, 2003) or laser–plasma K_α sources (Tillman *et al*., 1996).

In the last few years, the use of spherically bent Bragg crystals as dispersive elements in the soft X-ray region has been considered for both dense plasma diagnostics and X-ray applications (see Pikuz *et al*., 2004, and references therein). Bent crystals used in Laue configuration are also currently considered as tools to achieve monochromatic beams to be used in medical applications at higher energies (Dill *et al*., 1998).

When dealing with such crystals, ray-tracing simulations of the beam propagation in these experimental setups are often required, due to the strong aberrations involved in using bent surfaces. Ray-tracing simulations are also needed to model the pattern of the X-ray backlighting beam in imaging applications. As shown below, this pattern can be quite nonhomogeneous when line emission from a backlighter laser–plasma source occur in the useful energy range.

Address correspondence and reprint requests to: L. Labate, Intense Laser Irradiation Laboratory–IPCF (CNR), Pisa, Italy. E-mail: luca.labate@ipcf.cnr.it

In this article, ray-tracing simulations of a bent Bragg crystal-based optics for monochromatic imaging of thin samples and differential absorption μ-imaging applications will be discussed. After a short introduction on the underlying principles, a brief description of the ray-tracing code will be given, followed by the results of the simulations, in particular concerning the spatial resolution of the system and the pattern of the X-ray beam.

2. THE OPTICAL CONFIGURATION IN BRIEF

A detailed description of a typical experimental setup is beyond the scope of this article and can be found elsewhere (Gizzi *et al.*, 2004). A schematic configuration used to obtain an X-ray monochromatic beam is shown in Figure 1 and is based upon an idea proposed by Pikuz *et al.* (2001) and Sanchez del Rio *et al.* (2001). The technique can be thought of as a modification of the well-known projection radiography technique, obtained by inserting a spherically bent crystal between the object to be imaged and the detector to get a monochromatic image.

With reference to Figure 1, if an X-ray source is placed on the Rowland circle (i.e., the circle whose radius is half the curvature of the crystal) and the object is between the source and the crystal, a radiography of the object is obtained in a plane lying at a distance from the crystal given by

$$x = p_t + \frac{p_t p_s - p_t^2}{p_t + p_s}, \tag{1}$$

where p_t and p_s are the position of the tangential (horizontal) and sagittal (vertical) focuses respectively, given by the usual relations

$$\frac{1}{q} + \frac{1}{p_{t,s}} = \frac{1}{f_{t,s}}. \tag{2}$$

Here q is the distance from the center of the crystal to the source and f_t and f_s are the focal lengths of the crystal in the tangential and sagittal directions, respectively. If ϑ_0 is the glancing (Bragg) angle at the center of the crystal, the latter two quantities can be written as $f_t = R \sin \vartheta_0/2$ and $f_s = R/(2 \sin \vartheta_0)$. The object is "imaged" (actually, the object and image planes are not conjugated) at the plane given by Eq. (1) with a magnification factor $M = (x - p_t)/(q - x_o)$, where x_o is the distance from the crystal to the object. Due to the astigmatism of the system for working angles $\vartheta \neq \pi/2$, this is the only plane in which an undistorted (i.e., with the same magnification in the tangential and sagittal directions) transmission image can be obtained. This will be further clarified by the results of the ray-tracing simulations shown in Section 3.

The degree of monochromaticity of the beam used for the radiography is defined by the position of the X-ray source. In our case the source is placed on the Rowland circle, therefore providing a narrow dispersion curve along the crystal. Figure 2 shows the wavelengths diffracted in the case of a bent mica crystal ($2d = 19.9$ Å [Hölzer *et al.*, 1998], radius of curvature $R = 150$ mm) as a function of a curvilinear coordinate s along the crystal (in the horizontal plane), for a crystal size of 48 mm in the tangential plane. This behavior is defined by the usual Bragg relation:

$$\lambda(s) = \frac{2d}{n} \sin[\vartheta(s)]. \tag{3}$$

The calculation is performed for a glancing angle at the center of the crystal ($s = s_c = 0$) $\vartheta_c = \vartheta_{He\alpha} \simeq 0.8929$ rad and a diffraction order $n = 2$. These parameters give a central wavelength diffracted by the crystal $\lambda_c = \lambda_{He\alpha} \simeq 7.75$ Å, corresponding to the wavelength of the resonance line Heα ($1s2p$–$1s^2$ transition) from the He-like Al ions (unless otherwise specified, we will refer to these values for λ_c and ϑ_c from now on).

In the figure the three curves all refer to the source at an angle $\vartheta_{He\alpha}$ with respect to the crystal normal at its vertex,

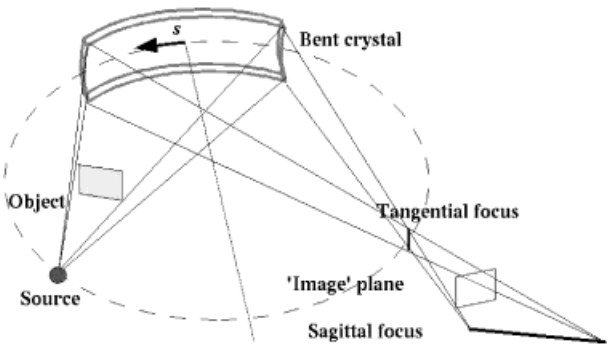

Fig. 1. Crystal optics setup for the the simulated experiment. The direction of a curvilinear coordinate s along the crystal is indicated.

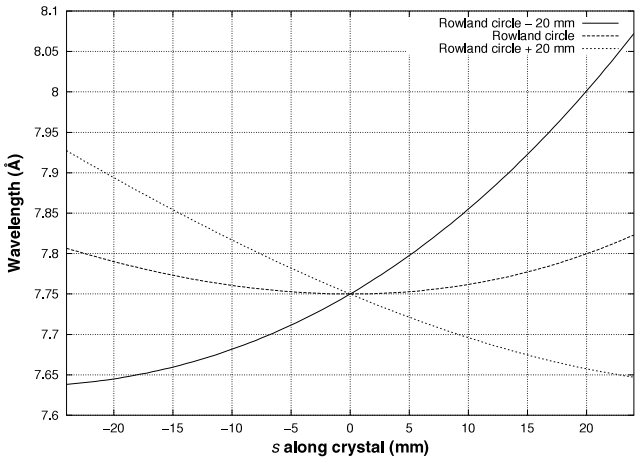

Fig. 2. Wavelengths diffracted by the bent crystal as a function of the coordinate s (see Fig. 1). Data are shown for three different positions of the source (see text), all referring to the same value of ϑ_c (see text).

but at different distances from the crystal surface; the dashed curve refers to the case in which the source is on the Rowland circle, the fine dashed one to the source placed 20 mm farther from the crystal, and the solid curve gives the result when the source is placed 20 mm closer to it. These plot clearly shows that when the source is on the Rowland circle a nearly monochromatic beam is diffracted, with a spectral width across the whole crystal length that, in the case taken into account, is about 50 mÅ, which gives a $\Delta\lambda/\lambda \simeq 7 \times 10^{-3}$ at $\lambda = 7$ Å. This enables a monochromatic transmission image of the object to be obtained in the image plane.

It is worthwhile noting that the flatness of the dispersion curve shown in Figure 2 in the case of the source placed on the Rowland circle also enables a nearly uniform X-ray beam pattern to be obtained in an illuminated field of some millimeters, regardless of the fact that the source exhibits a continuous or line emission. This issue, which is quite important for imaging purposes, will be clarified and confirmed by the ray-tracing results.

3. RAY-TRACING SIMULATIONS

In this section we illustrate the results of ray-tracing of the simulated experiment of Figure 1, performed using the code ORTO (an Object-oriented Ray-Tracing envirOnment) developed for this purpose at the Intense Laser Irradiation Laboratory (ILIL). The geometrical features of different optical setups based on bent Bragg crystals, as well as other optical elements, can be modeled by the code, which is also able to consider the physical characteristics of the interaction with the crystal by taking into account the crystal rocking curve. The code generates, using a Monte Carlo method, a set of rays originating in a given region of the space with a user-defined density and propagating toward another region with a suitable angular distribution. The spectral distribution of the source can also be considered.

The code is written in C++ language; it contains five major objects, which are inherited by other classes: `ORTOsource`, `ORTOobstacle`, `ORTOdetector`, `ORTOray`, `ORTOsetup`. The first three objects are abstract classes declaring the pure virtual functions `RayGun()`, `Interaction()`, and `Detection()`, which perform the fundamental operations of the ray-tracing; these functions are then overridden in the derived classes such as `ORTOsphericalcrystal` or `ORTOZonePlate` (see below). A detailed description of the code structure is beyond the scope of this report: We only mention here the fact that, unlike the SHADOW code (Welnak *et al*., 1994), the *de facto* standard code for synchrotron radiation applications (Cerrina *et al*., 1996), a ray has not a unique value of the photon energy, but is defined by its origin and its direction only. The physical characteristics of each ray are taken into account by a *path*, which contains $N_{obst} + 1$ (N_{obst} is the number of obstacles) rays; it also contains the variables defining the spectrum of the source and it keeps track of the interaction with each obstacle in order to modify the initial spectrum (the functions that calculate the final spectrum are defined inside the class `ORTOpath`; to improve the execution speed, pointers to these [member] functions are then passed to the functions performing the detection by each detectors).

Simulations by ORTO were performed to model the optical properties of the setup of Figure 1. Because the first experimental setup trials were carried out for differential imaging across the $L_2 2p_{1/2}$ edge of Br at 1596 eV (see the website at http://physics.nist.gov/PhysRefData), here we report the results obtained with a glancing angle at the center of the crystal $\vartheta_c \simeq 0.8921$ rad, corresponding to a diffracted wavelength $\lambda_c \simeq 7.745$ Å ($E \simeq 1600$ eV), just above the Br edge.

The spectrum of the laser–plasma point source was supposed, on the basis of previous experiments performed in the same target irradiation conditions (Labate *et al*., 2001), as consisting of two Gaussian lines centered at $\lambda_1 = 7.75$ Å and $\lambda_2 = 7.80$ Å, with HWHM $\Delta\lambda_1 = \Delta\lambda_2 = 5$ mÅ and intensity $A_1 = 10A_2$, corresponding to the *Heα* and to the IC line from He-like Al ions, respectively.

Although more general forms of rocking curves can be considered by ORTO, the crystal rocking curve was taken into account in the simplified form

$$R(\lambda - \lambda_i) = \begin{cases} 1 & \text{for } |\lambda - \lambda_i| \le \Delta\lambda_r \\ 0 & \text{elsewhere,} \end{cases} \tag{4}$$

where λ_i is the wavelength corresponding to the angle of incidence of the ray on the crystal and $\Delta\lambda_r$ is half the width of the rocking curve as given by Sanchez del Rio *et al*. (2000).

Unless otherwise stated, the simulations described below were all performed taking into account a point source. This source was considered to generate, using a Monte Carlo method, 10^6 rays per run, with isotropic angular distribution, toward the crystal. Typical running times were in the range 2–4 min on a Pentium II 400MHz CPU with a Linux operating system.

Figure 3 shows the radiation intensity detected assuming a CCD-like detector with an array of 26.4×7.9 mm^2 size, 1100×330 pixels, like the one used in Gizzi *et al*. (2004), placed in the position of the image plane (see Fig. 1). As above, the crystal is supposed to be 48×12 mm^2 wide. The coordinate s in the figure identifies vertical slabs of the detector illuminated by different parts of the crystal, whose coordinate is as in Figure 1: s_0 and s_1 indicate the two boundaries of the crystal ($s = -24$ mm and $s = +24$ mm in Fig. 1) and s_c corresponds to the center of the crystal ($s = 0$ mm in Fig. 1). The overall shape of the illuminated field is due to the dependence of the sagittal focal length of the crystal upon the angle of incidence, which results in different heights in the plane of the detector. The main spectral component in the figure is the *Heα* line, reflected by the central region of the crystal where, as pointed out above, a

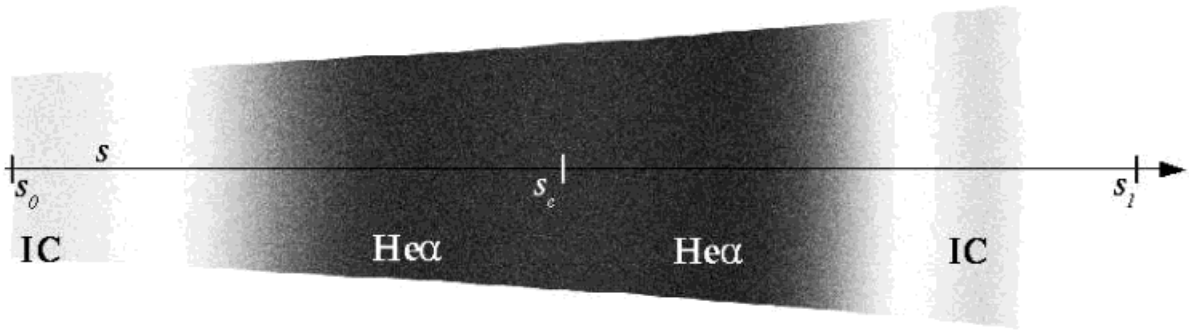

Fig. 3. Radiation intensity detected by a 26.4×7.9-mm^2 size, 1100×330-pixels detector in the position of the image plane as obtained by ORTO simulations with 10^6 sampled rays (darker gray levels correspond to brighter regions of the X-ray beam). The coordinate s identifies slabs of the detector illuminated by different regions of the crystal as is in Figure 1.

nearly flat behavior of the dispersion curve occurs (see Fig. 2). Toward the left and right edges of the detector the two weaker components (coming from two distinct regions of the crystal nearly symmetric with respect to its center) due to the IC line are also clearly visible.

To test the imaging properties of the configuration, ray-tracing simulations were performed considering a Fresnel zone plate as an object to be imaged out. In our experiment (Gizzi *et al.*, 2004) this plate is used as a resolution test sample due to its well-known spatial properties. The zone plate taken into account had $\lambda f = 1.14 \times 10^{-1}$ mm^2, resulting in a radius of the first opaque zone $r_1 = \sqrt{\lambda f} \simeq 340$ μm, and a total radius of 3.5 mm. The zone plate was placed along the direction joining the source and the crystal, at a distance from the source chosen so as to get a magnification $M \simeq 1.6$. Figure 4 shows the radiation detected by the same planar detector as in Figure 3, placed in the image plane. Similar results were also obtained for the detector closer to the crystal by 1 cm (Fig. 5) and farther from the crystal by the same amount (Fig. 6). The latter two figures provide clear visual and quantitative proof of the fact that the image plane defined by Eq. (1) is the only one where a radiography is obtained preserving the aspect ratio of the object.

The spatial resolution attainable using the scheme described above has also been studied by performing ray-tracing simulations with a finite size backlighting source. To this purpose, a planar source with a Gaussian shape has been used. Each ray thus has its origin on a plane normal to the line joining the source and the center of the crystal; the probability for this origin to be at a distance r from the source center is given by a Gaussian distribution (having its maximum at $r = 0$).

Figure 7 shows the intensity distribution on a planar detector when a mesh with period 300 μm and wire thickness 50 μm is used as a test object to be imaged (the wires are supposed completely opaque to the X-ray radiation). The source size is 30 μm FWHM and the spectrum is the same as that of Figure 3. A lineout of the image of Figure 7 along the horizontal (tangential) direction is shown in Figure 8, performed near to the center of the image (i.e., to the tangential plane of the system). The overall structure of the backlighting X-ray beam (corresponding to the image of Fig. 3) due to its line structure is clearly visible in this plot, together with the superimposed structure of the imaged mesh. From the lineout of Figure 8 the spatial resolution of the bent-crystal-based optical system in the horizontal direc-

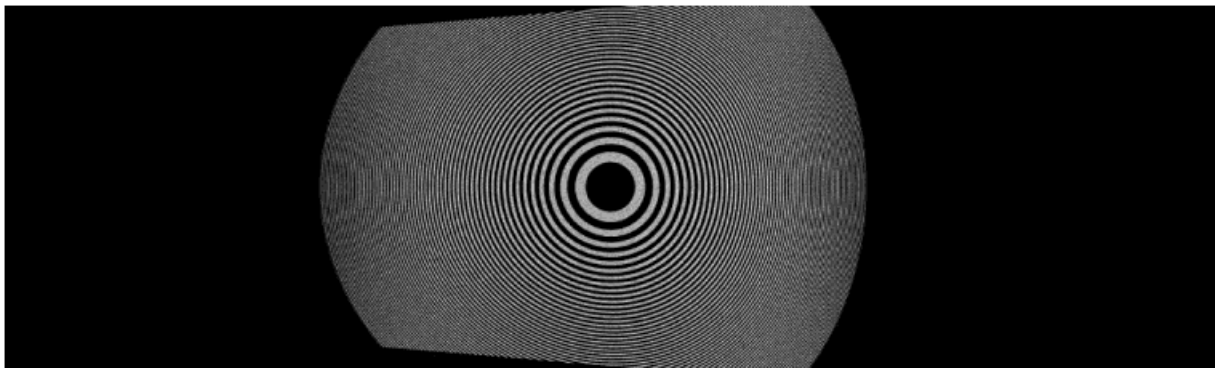

Fig. 4. Image of a Fresnel zone plate provided by a planar detector in the image plane, as obtained by ORTO with 10^6 sampled rays (darker gray levels correspond to a smaller X-ray intensity).

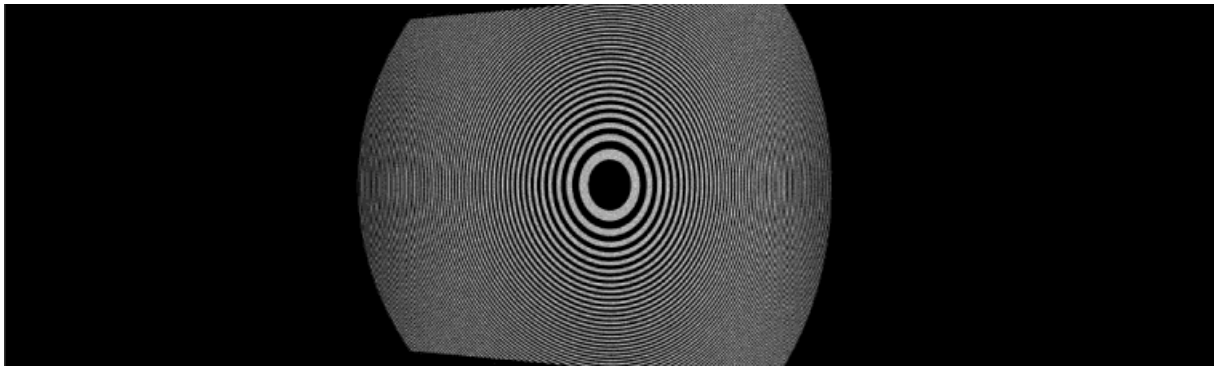

Fig. 5. Image of a Fresnel zone plate provided by a planar detector closer to the crystal by 1 cm with respect to the image plane, as obtained by ORTO with 10^6 sampled rays.

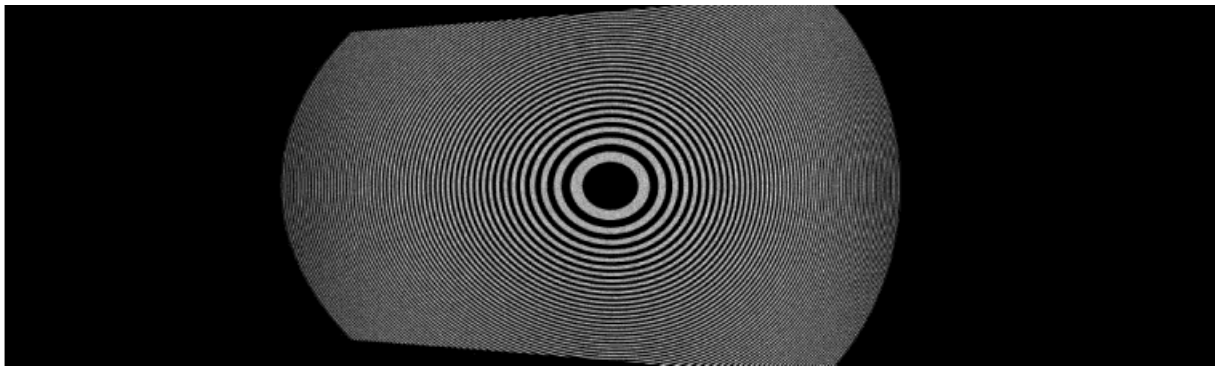

Fig. 6. Image of a Fresnel zone plate provided by a planar detector farther from the crystal by 1 cm with respect to the image plane, as obtained by ORTO with 10^6 sampled rays.

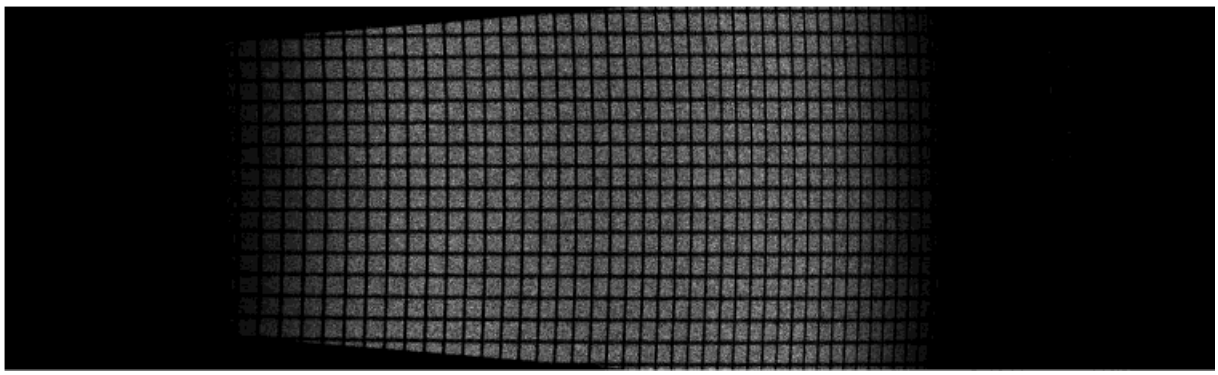

Fig. 7. Image of a 300-μm period, 50-μm wire thickness mesh, with a magnification $M = 1.6$, provided by a detector in the image plane, as obtained by ORTO with 10^6 sampled rays.

tion can be estimated, by considering the width of the transition region from an illuminated to an opaque zone corresponding to a wire of the mesh. In such a way, a horizontal resolution of about 15 μm in the plane of the object has been estimated. A similar procedure enabled us to find a worse resolution of about 40 μm in the vertical direction.

Such a poor resolution in the vertical direction is actually the main drawback of using the scheme presented to perform monochromatic imaging. To improve the resolution, both horizontal and vertical, of a monochromatic imaging setup based on spherically bent crystals, slightly different schemes have recently been proposed (Pikuz *et al.*, 2004).

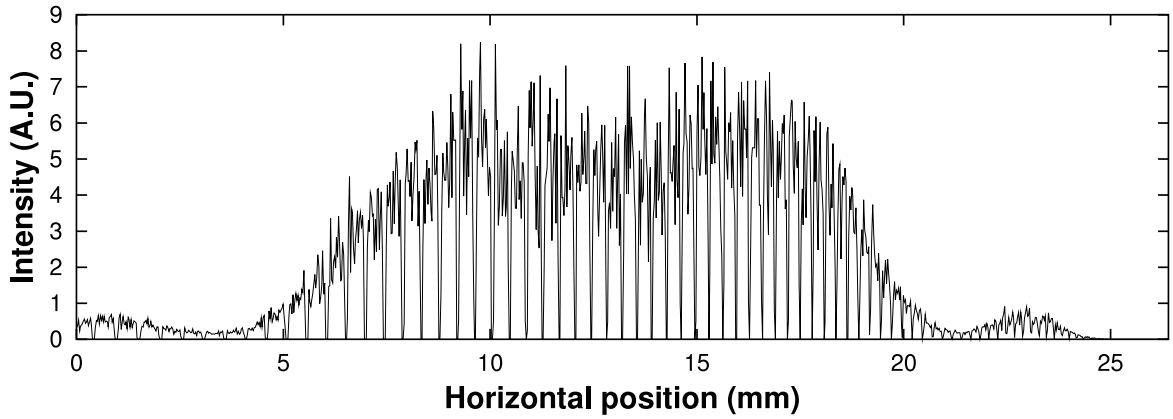

Fig. 8. Lineout of the image of Figure 7 along the horizontal (tangential) direction, performed near to the center of the image (i.e., near the tangential plane of the system).

4. CONCLUSIONS AND PERSPECTIVES

We reported here on the ray-tracing simulations of an experimental setup, based on a spherically bent mica crystal, devoted to obtaining monochromatic microradiographies of thin samples using a laser–plasma source. In particular, results by the code ORTO, recently developed at ILIL, were shown. The spatial resolution attainable using this kind of optical system has been estimated by performing simulations with a finite size source. The complex structure of the backlighting X-ray beam, due to a line spectrum of the source and to the features of the dispersion curve across the crystal, has been carefully studied. The simulations demonstrate the capability of ORTO to geometrically model simple experimental arrangements with bent Bragg crystals. Further efforts are currently going on devoted to the improvement of the code capabilities, in particular with respect to the physical model describing the X-ray diffraction from the Bragg crystals.

ACKNOWLEDGMENTS

We would like to thank A. Barbini, A. Rossi, A. Salvetti, W. Baldeschi, and M. Voliani for their invaluable technical assistance. SL acknowledges financial support from the European Research Training Network XPOSE Contract No. HPRN-CT-2000-00160. LL and PT acknowledge financial support from MIUR (Project "Metodologie e diagnostiche per materiali ed ambiente"). This work was partially supported by the MIUR Project "Impianti innovativi multiscopo per la produzione di radiazione X."

REFERENCES

Bastiani, S., Rousse, A., Geindre, J.P., Audebert, P., Quoix, C., Hamoniaux, G., Antonetti, A. & Gauthier, J.C. (1997). Experimental study of the interaction of subpicosecond laser pulses with solid targets of varying initial scale lengths. *Phys. Rev. E* **56**, 7179–7185.

Burattini, E., Gambaccini, M., Indovina, P.L., Marziani, M. & Rimondi, O. (1990). S/N ratio evaluation in synchrotron radiation radiography. *Phys. Med.* **21**, 1853–1863.

Cerrina, F., Hulbert, S.L. & Sanchez del Rio, M. (1996). Summary of the workshop on "X-ray optics and ray-tracing: Status and needs." *Rev. Sci. Instrum.* **67**, 1–2.

Dill, T., Dix, W.-R., Hamm, C.W., Jung, M., Kupper, W., Lohmann, M., Reime, B. & Ventura, R. (1998). Intravenous coronary angiography with synchrotron radiation. *Eur. J. Phys.* **19**, 499–511.

Dix, W.-R. (1995). Intravenous coronary angiography with synchrotron radiation. *Prog. Biophys. Molec. Biol.* **63**, 159–191.

Giulietti, D. & Gizzi, L.A. (1998). X-ray emission from laser-produced plasmas. *Riv. Nuovo Cimento* **21**, 1–93.

Gizzi, L.A., Cecchetti, C.A., Galimberti, M., Giulietti, A., Koester, P., Labate, L., Laville, S. & Tomassini, P. (2004). Differential absorption imaging of thin samples using a laser–plasma soft X-ray source. *Laser Part. Beams* **22**, xxx–xxx.

Hölzer, G., Wehrhan, O., Heinisch, J., Förster, E., Pikuz, T.A., Faenov, A.Ya., Pikuz, S.A., Romanova, V.M. & Shelkovenko, T.A. (1998). Flat and spherically bent muscovite (mica) crystals for X-ray spectroscopy. *Phys. Scripta* **57**, 301–309.

Labate, L., Galimberti, M., Giulietti, A., Giulietti, D., Gizzi, L.A., Numico, R. & Salvetti, A. (2001). Line spectroscopy with spatial resolution of laser–plasma X-ray emission. *Laser Part. Beams* **19**, 117–122.

Labate, L., Galimberti, M., Giulietti, A., Giulietti, D., Gizzi, L.A., Tomassini, P. & Di Cocco, G. (2002). A laser–plasma source for CCD calibration in the soft X-ray range. *Nucl. Instr. Meth. A* **495**, 148–152.

Marzi, S., Giulietti, A., Giulietti, D., Gizzi, L.A. & Salvetti, A. (2000). High brightness laser–plasma X-ray source at IFAM: Characterization and applications. *Laser Part. Beams* **18**, 109–118.

Pikuz, T.A., Faenov, A. Ya., Fraenkel, M., Zigler, A., Flora, F., Bollanti, S., Di Lazzaro, P., Letardi, T., Grilli, A., Palladino, L., Tomassetti, G., Reale, A., Reale, L., Scafati, A., Limongi, T., Bonfigli, F., Alianelli, L. & Sanchez del Rio, M. (2001). Shadow monochromatic back-

lighting: Large-field high resolution X-ray shadowgraphy with improved spectral tunability. *Laser Part. Beams* **19**, 285–293.

Pikuz, T.A., Faenov, A., Skobelev, I., Magunov, A., Labate, L., Gizzi, L.A., Galimberti, M., Zigler, A., Baldacchini, G., Flora, F., Bollanti, S., Di Lazzaro, P., Murra, D., Tomassetti, G., Ritucci, A., Reale, A., Reale, L., Francucci, M., Martellucci, S. & Petrocelli, G. (2004). Easy spectrally tunable high efficient X-ray backlighting scheme based on the spherically bent crystals. *Laser Part. Beams* **22**, xxx–xxx.

Reich, Ch., Gibbon, P., Uschmann, I. & Förster, E. (2000). Yield optimization and time structure of femtosecond laser plasma Kα sources. *Phys. Rev. Lett.* **84**, 4846–4849.

Sanchez del Rio, M., Faenov, A.Ya., Pikuz, T.A., Souvorov, A. & Freund, A.K. (2000). Hard X-ray reflectivity of spherically bent mica crystals. *AIP Conference Proceedings* **521**, 287–292.

Sanchez del Rio, M., Alianelli, L., Pikuz, T.A. & Faenov, A.Ya. (2001). A novel imaging X-ray microscope based on a spherical crystal. *Rev. Sci. Instrum.* **72**, 3291–3303.

Suortti, P. & Thomlinson, W. (2003). Medical applications of synchrotron radiation. *Phys. Med. Biol.* **48**, R1-R35.

Tillman, C., Mercer, I., Svanberg, S. & Herrlin, K. (1996). Elemental biological imaging by differential absorption with a laser-produced X-ray source. *J. Opt. Soc. Am. B* **13**, 209–215.

Von Der Linde, D., Sokolowski-Tinten, K., Blome, Ch., Dietrich, C., Zhou, P., Tarasevitch, A., Cavalleri, A., Siders, C.W., Barty, C.P.J., Squier, J., Wilson, K.R., Uschmann, I. & Förster, E. (2001). Generation and application of ultrashort X-ray pulses, *Laser Part. Beams* **19**, 15–22.

Welnak, C., Chen, G.J. & Cerrina, F. (1994). SHADOW: A synchrotron radiation and X-ray optics simulation tool. *Nucl. Instr. Meth. A* **347**, 344–347.